UNIVERSITY OF LEEDS

This is a repository copy of *Dynamic Response of Circulation Control for Step and Sinusoidal Inputs*.

White Rose Research Online URL for this paper:
https://eprints.whiterose.ac.uk/198642/

Version: Accepted Version

Article:
Li, S and Shires, A orcid.org/0000-0001-6523-2636 (2023) Dynamic Response of Circulation Control for Step and Sinusoidal Inputs. Journal of Aircraft. ISSN 0021-8669

https://doi.org/10.2514/1.c037042

© 2023 by the American Institute of Aeronautics and Astronautics, Inc. This is an author produced version of an article published in Journal of Aircraft. Uploaded in accordance with the publisher's self-archiving policy.

Reuse
Items deposited in White Rose Research Online are protected by copyright, with all rights reserved unless indicated otherwise. They may be downloaded and/or printed for private study, or other acts as permitted by national copyright laws. The publisher or other rights holders may allow further reproduction and re-use of the full text version. This is indicated by the licence information on the White Rose Research Online record for the item.

Takedown
If you consider content in White Rose Research Online to be in breach of UK law, please notify us by emailing eprints@whiterose.ac.uk including the URL of the record and the reason for the withdrawal request.

White Rose university consortium
Universities of Leeds, Sheffield & York

eprints@whiterose.ac.uk
https://eprints.whiterose.ac.uk/

The dynamic response of circulation control for step and sinusoidal inputs

Shaoze Li *, Andrew Shires†
University of Leeds, Leeds, LS2 9JT

A numerical study of the dynamic performance of a circulation controlled (CC) aerofoil is performed to explore the feasibility of using CC as means of gust suppression. Steady and unsteady two-dimensional Computational Fluid Dynamic (CFD) simulations were initially validated using published data. The dynamic performance of a CC aerofoil was subsequently assessed. The response of the CC aerofoil to step and sinusoidal inputs were obtained from unsteady CFD simulations. It was found that the actuation speed of CC is significantly faster than a conventional mechanical flap at the same flight condition. Additionally, the lift response to a step input was found to be very similar to the Küssner function.

Nomenclature

c	=	chord, m
Re	=	free-stream Reynolds number
C_L	=	lift coefficient
C_μ	=	jet momentum coefficient
h	=	jet slot height, m
w	=	slot width, m
b	=	span, m
ρ_J	=	jet density, kg/m^3
ρ_∞	=	free stream density, kg/m^3
U_J	=	jet velocity, m/s
U_∞	=	free stream velocity, m/s
γ	=	heat capacity ratio
R	=	gas constant
T	=	static temperature, K
P_∞	=	free stream pressure, Pa

*PhD student, School of Mechanical Engineering.
†Associate Professor, School of Mechanical Engineering.

P_{tJ} = jet total pressure, Pa

NPR = nozzle pressure ratio

q = dynamic pressure, Pa

w_g = gust velocity, m/s

s = nondimensional time 2t*U/c

s' = nondimensional time t*U/c

I. Introduction

The market for Civilian Unmanned Aerial Vehicles (UAVs) is ever expanding with a wide range of potential missions such as; logistics, surveillance, mapping, inspection, photography, search and rescue etc. Since fixed-wing UAVs typically have a smaller weight and inertia than manned aircraft, their stability and control is more sensitive to medium and high frequency changes in wind speed and direction i.e. gusts and turbulence. Additionally, since UAV's are being tasked with flying at lower altitudes than manned aircraft they are more likely to encounter terrain-induced weather features such as katabatic wind or turbulence. This research assesses the feasibility of active flow control to alleviate the potential hazards of wind gusts and turbulence for UAVs.

An aircraft's response to a gust relates to its change in wing loading or load factor [1], which for a sharp-edged gust is given by;

$$\Delta n = C_{L_\alpha} \frac{\rho u_0}{2} \frac{A_g}{W/S} \tag{1}$$

where Δn is the load factor (i.e., the ratio of maximum vertical acceleration to the gravitational constant $\Delta n = \Delta \dot{w}/g$), C_{L_α} is the lift curve slope of the aircraft, ρ is the air density, u_0 is the flight velocity, A_g is the normal velocity component of the gust, and W/S is the wing loading. This equation indicates that an aircraft with a lower wing loading is more sensitive to a wind gust. Due to their mission requirement, the wing loading of small and low speed UAVs is usually lower than large commercial or high-speed aircraft [2]. Consequently, their vertical acceleration and wing root bending moment due to a vertical gust are generally more severe. The statistical distribution of gust intensity has been modelled by von Karmen and Dryden [3]. In the frequency domain, the power spectra of turbulence velocity depends on the distance to the ground, surface wind and flight speed. Whereas the power spectra of aircraft response, especially the harmonic frequency, is mainly affected by the inherent dynamic characteristics of the specific aircraft. The peak response of vertical acceleration is near the short period mode of the aircraft which is normally in the range of 10^0 to 10^1 rad/s [1][3]. The high frequency gust is sufficiently attenuated. Consequently the present study is mainly focused on the frequency range 3.14-314 rad/s, which covers the short period mode of a rigid body and the structural mode due to aeroelastic effects.

Large civil aircraft typically use gust load alleviation (GLA) systems to counteract local lift changes caused by vertical wind gusts. This reduces the maximum wing root bending moment and collective cyclic loads (and therefore fatigue) on the primary structure, allowing for potential weight reductions and longer inspection intervals. The effects of longitudinal and lateral wind gusts are also detected and alleviated but have a lesser effect on performance. Furthermore, vertical motion has a greater impact on passenger comfort and pilot reactions [4] if not alleviated. The systems work by measuring the vertical acceleration of the aircraft using accelerometers located in the fuselage and wings, relative to any acceleration commanded by the (auto)pilot. A feedback controller adds a correction to the signal controlling the deflection of conventional control surfaces (ailerons, elevators and spoilers) in order to alter the lift and thereby counteract the accelerations caused by wind gusts. Due to the relatively large mass and inertia of these aircraft they are more resistant to the wind gusts. More recently LIDAR[5] and surface pressure sensors are being used to provide earlier detection of gusts so that feedforward controllers can provide more effective GLA, such as that patented by Boeing [6]. For aircraft with a lower inertia such as general aviation and UAV's there is a need to increase the control authority and bandwidth for GLA to be effective. This paper considers active circulation control (CC) as a means of GLA for a wing incorporating a pneumatic (CC) aileron compared with a conventional mechanical aileron, and explorer the dynamic response of both methods.

Conventional control surfaces modify the lift by rotating the trailing-edge to change wing camber. In comparison, CC has no moving parts and uses an air jet to modify the location of the rear stagnation point. The principle of CC has been widely investigated as a potential alternative to conventional control surfaces for high lift or manoeuvring flight [7–17]. The wing trailing-edge shape is modified with an upper and lower surface nozzle through which a jet sheet is introduced tangentially to a curved Coanda surface [18]. This jet sheet entrains and turns the external flow, delaying the rear stagnation point relative to a conventional sharp trailing-edge, thereby increasing the circulation around the wing and thus lift. The lift increment is a function of the relative speed of the jet sheet (and therefore the nozzle pressure ratio), as well as the nozzle height and Coanda surface curvature [18]. Whilst previous research has focused on steady state CC [8, 9, 11, 19–25], the present study investigates its dynamic performance in order to evaluate potential actuation speeds and compare bandwidth with conventional mechanical actuators. Its dynamic performance will also determine the design of the control algorithm.

The dynamic response of conventional aerofoils with mechanical actuators has been widely investigated [26–34]. Ghoreyshi and Cummings reported indicial responses of control surfaces for step, ramp and sinusoidal signals [30]. Seidler et al. investigated a surrogate model for the prediction of response, which is less expensive compared to Reynolds-Averaged Navier Stokes equations [32]. Carlsson [29] and Phillips [34] performed experimental tests of transient deployment of mechanical control surfaces.

Several studies have reported on the dynamic response of flow control which includes synthetic jets and pulsed blowing[35–37]. Kerstens et al.[37] studied gust suppression with pulsed blowing arrays using a wind tunnel equipped

with a gust generator to develop unsteady flow conditions. The wing loads were sensed using a six-component balance and the gust information was measured with a hotwire anemometer. The resulting unsteady loading was suppressed by adjusting a leading-edge flow control device using a closed-loop feedback controller. In terms of CC, studies on its dynamic response are still rare. Friedman and Arieli investigated the lift build-up process of CC [38], suggesting that the lift variation is similar to a Wagner function. Li et al. investigated the application of CC for gust alleviation [39]. However their research did not include frequency variation which is important for the analysis of flight mechanics, and there was no comparison with conventional aerodynamic surfaces. The present study uses the Ansys Fluent version 19.2 Computational Fluid Dynamics (CFD) package [40], solving the unsteady compressible Reynolds-Averaged Navier Stokes (URANS) equations. Step response and frequency response of CC were conducted, and the response time and bandwidth were compared with conventional aerodynamic surfaces.

The paper initially describes a steady CFD validation of an existing CC-aerofoil using published experimental data [41] in section 2. Subsequently an unsteady validation is described in section 3. The frequency response of this aerofoil is reported in section 4 for dynamic free stream conditions and nozzle boundary conditions. Its dynamic performance is then compared with a conventional mechanical aileron in section 4 in terms of actuation speed and effectiveness. Finally, concluding remarks are given in section 5.

II. Steady state validation

A. The General Aviation Circulation Control (GACC) aerofoil

The study uses the existing General Aviation Circulation Control (GACC) aerofoil developed by Jones et al. [41] and shown in Fig. 1. The GACC aerofoil was modified from the GAW-1 aerofoil, a low-speed 17% thick aerofoil, by transforming its sharp trailing edge to a circular Coanda surface, as shown in the blue dashed line in Fig. 1. A backward facing step is located on both the upper and lower side of the Coanda surface with a dimension of $h/c = 0.0011$, where h is the step height and c is the aerofoil chord. In the present study only the upper step is used as a jet exit for CC. An internal plenum chamber is located upstream of the jet exit that supplies high pressure air to a convergent nozzle. Except for the modifications to the trailing edge, the remaining aerofoil shape is the same as the GAW-1 aerofoil.

A GACC model was tested in the Basic Aerodynamics Research Tunnel in Langley Research Center by Jones et al. [41] to obtain lift increments and surface pressure distributions for different angles of attack and nozzle pressure ratios. In the present study a 2-D CFD analysis of this aerofoil was conducted with and without blowing to validate the mesh and physics approach, by comparing results with those from the experiment.

The free stream Mach number in the present study is less than 0.2 and the jet velocity at the nozzle exit is less than Mach 0.5. Thus, the flow is mildly compressible so the pressure based compressible solver is used and the SIMPLE (Semi-implicit Method for Pressure Linked Equations) algorithm is selected to solve the pressure-velocity coupling

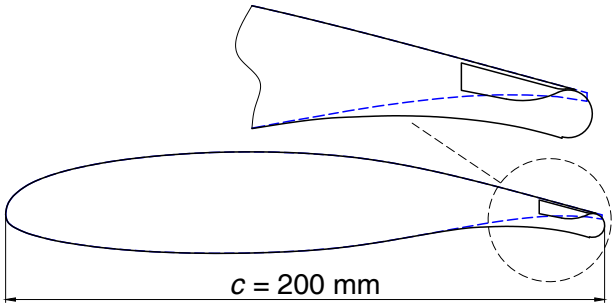

Fig. 1 The geometry of the General Aviation Circulation Control (GACC) aerofoil compared with the original GAW-1 aerofoil shown in dashed blue line

problem. An ideal-gas is assumed with an initial temperature of 288K. In terms of the discretization approach, a second order upwind finite volume method is used for spatial discretization and the second order implicit method is used for temporal discretization.

B. Mesh and boundary conditions

A common parameter used to quantify blowing for CC is the momentum coefficient (C_μ) given by equation 2, where h and w are the nozzle height and width respectively, b is the wing span but in this 2D case, $w = b = 1$. The ρ and U are the density and velocity of the fluid, while the subscript ∞ denotes the free stream conditions, and J is the blowing jet conditions. Since the nozzle exit velocity is not uniform (as shown in Fig. 11 (left)), and the nozzle height is typically very small, C_μ is difficult to measure experimentally [13]. Therefore blowing is more conveniently defined by the nozzle pressure ratio (NPR) given by equation 3, where P_{tJ} is the plenum stagnation pressure and P_∞ is the freestream static pressure. Assuming an isentropic flow through the convergent nozzle the mean jet exit velocity U_J can be determined using equation 4, where γ is the heat capacity ratio, R is the gas constant, and T is the static temperature.

$$C_\mu = \frac{2hw}{cb}\frac{\rho_J}{\rho_\infty}\frac{U_J^2}{U_\infty^2} \tag{2}$$

$$NPR = P_{tJ}/P_\infty \tag{3}$$

$$U_J = \sqrt{\frac{2\gamma RT_{tJ}}{\gamma - 1}\left[1 - \left(\frac{P_\infty}{P_{tJ}}\right)^{\frac{\gamma-1}{\gamma}}\right]} \tag{4}$$

Fig. 2 displays the dimensions of the plenum chamber, nozzle exit and Coanda surface radius for an aerofoil chord of 200 mm. A stagnation inlet boundary condition was applied to the plenum chamber face highlighted by the red line in Fig. 2. The NPR was calculated using Equations 2 - 4 corresponding to the C_μ published for the experimental data. Although a uniform velocity inlet boundary condition could be used to establish the jet flow as in [42] the majority of previous researches included the plenum chamber to give a more representative jet velocity profile due to

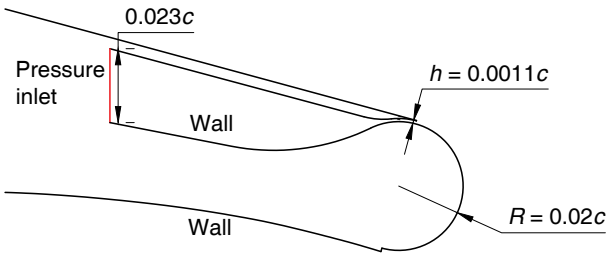

Fig. 2 Boundary conditions and dimensions of the nozzle.

the development of boundary-layers within the plenum.

Flow solutions for these analyses were performed at a freestream Mach number of 0.1 assuming sea level International Standard Atmosphere (ISA) conditions and 0° angle of attack (AoA). The chord Reynolds number of Re = 4.6×10^5 matches that of the experiment [40]. The boundary condition of the nozzle inlet was set to be a pressure inlet, and a no-slip condition was used for aerofoil and plenum chamber surfaces. The thickness of the first layer adjacent to the wall was 0.012mm to keep the Wall y+ less than 1. To model the free-stream condition, a pressure far field was used and dynamically controlled by pre-defined scripts. Structured meshes were generated using ANSYS ICEM. Through refinement the number of cells increased from 86,211 to 211,811 as shown in Fig. 3, where the percentage error is relative to the lift for the finest mesh level.

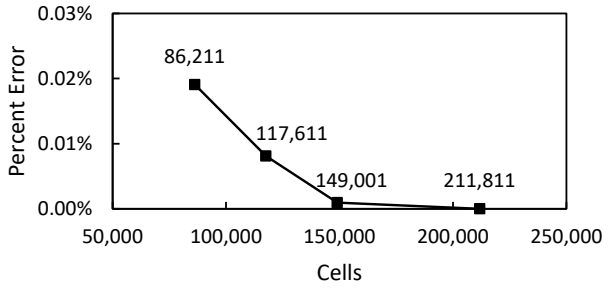

Fig. 3 The variation of lift coefficient over increasing mesh density. M_∞ = 0.1, AoA = 0°.

The mesh density in the vicinity of the Coanda jet is one of the factors that influence the simulation accuracy of CC. In Fig. 4, the pressure distribution around the Coanda surface using different meshes were compared to ensure that the separation point is independent of mesh density. The difference between various meshes was indistinguishable.

According to the lift result and the pressure distribution, the mesh containing 149,001 cells was shown to give a mesh independent result in terms of an acceptable accuracy of lift coefficient, and has therefore been used for all further CFD analyses. Fig. 5 illustrates the corresponding mesh and the refinement added to capture interactions between the jet and external flow streams.

A sensitivity study to the domain size was also conducted with far field distances of 10c, 25c, and 100c at $C_\mu = 0.015$.

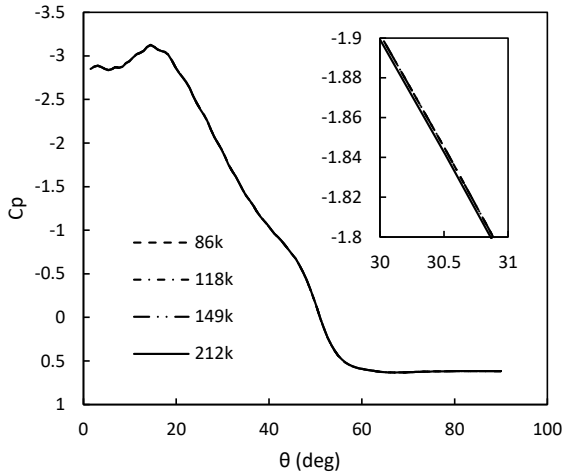

Fig. 4 The pressure distribution around the Coanda surface using different meshes, the inset graph shows a close-up view of the curve. C_μ = 0.015, M_∞ = 0.1, AoA = 0°.

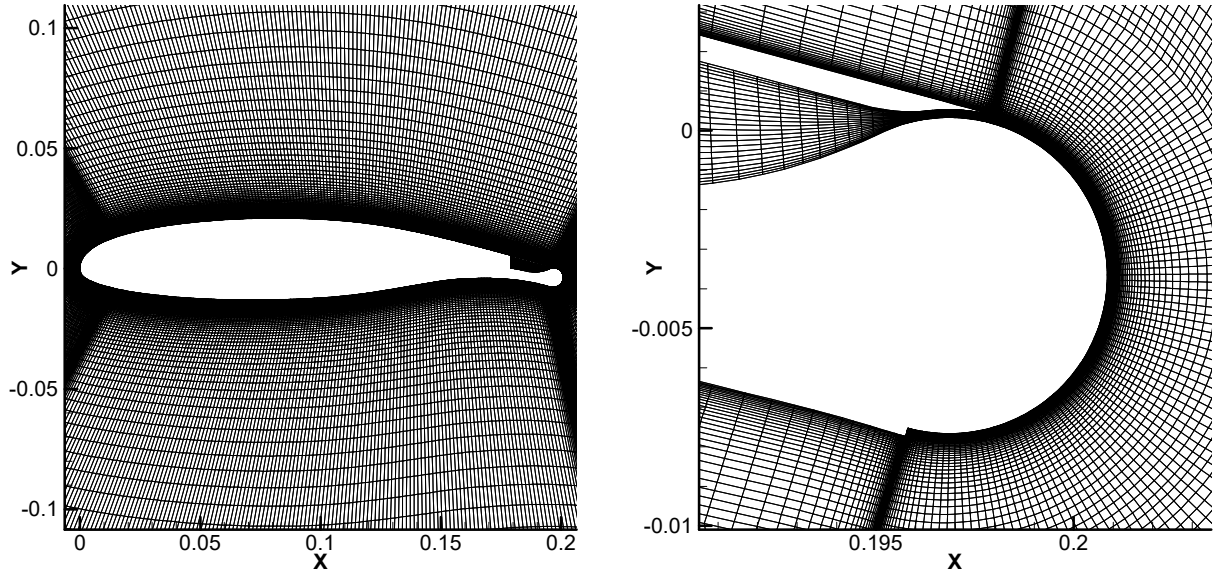

Fig. 5 The mesh of the geometry, left: mesh around the aerofoil, right: mesh around the trailing edge.

Resulting pressure distributions are shown in Figure 6. It was found that domain size only has a minor influence on the suction peak pressure around the Coanda surface as shown in the expanded view. A distance of 25c was therefore used for the study since it gave a very similar result to the 100c domain size.

C. Validation result

CFD simulations were performed at the NPRs given in Table 1 corresponding to the C_μ range 0 to 0.06 used in the experiment [41].

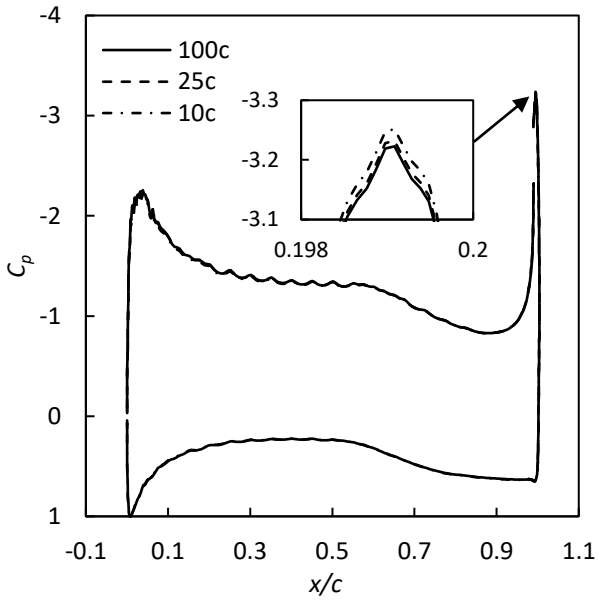

Fig. 6 Sensitivity study for far field distance of 10, 25, 100 chord length.

Table 1 Stagnation pressure in the plenum chamber for various blowing momentum coefficients (Reference pressure: 101325Pa, T = 293K, γ = 1.4, R = 287, q = 688.5Pa, AoA = 0°).

C_μ	U_J(m/s)	P_{tJ}(Pa)	NPR
0.015	91.8	107283	1.052
0.025	118.5	111000	1.088
0.04	149.9	116894	1.146
0.06	183.6	125394	1.229

Due to the high relative jet velocity and the complex shear flow that results, as well as the boundary-layer separation/reattachment mechanism around the Coanda surface, the prediction of circulation control using CFD is a significant challenge [40]. A workshop to evaluate appropriate meshing, boundary condition, turbulence model and solver strategies for CC [40] recommended three standard turbulence models: $k-\varepsilon$, $k-\omega$ SST and Spalart-Allmaras (SA). Each of these was evaluated for the range of cases given in Table 1 and results compared with experiment. The SA model was found to predict a higher lift coefficient and lower drag coefficient than both $k-\varepsilon$ and $k-\omega$ models which gave similar results. The SA model gives the highest deviation compared to the experimental C_L at NPR = 1.4. However, the rear stagnation position predicted with the SA model most closely matched the experimental result.

A further comparison of the $k-\omega$ and SA models was made with steady blowing, C_μ = 0.025, over the range of AoA 0° to 10° as shown in Fig. 7. The SA model gives a lift coefficient that more closely matches the measured value with a maximum difference of 4.5% at AoA = 10°. Although the $k-\omega$ model predicts a better trend compared with experiment it gives a lower lift coefficient, and since the following analyses are all performed at zero AoA, the SA model was selected.

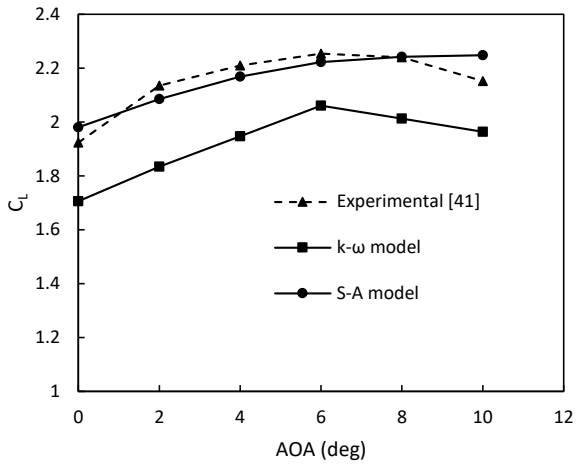

Fig. 7 Comparison between $k-\omega$ model, Spalart-Allmaras model and experimental data. ($C_\mu = 0.025$, M_∞ = **0.1, Re =** 4.6×10^5)

The GACC aerofoil performance was evaluated over the range of momentum coefficients given in table 1 for AoA = 0° and using the SA turbulence model. Fig. 8 compares the results obtained from CFD with the experiment. The figure shows that significant increments in C_L can be achieved using CC and that CFD is effective at predicting these increments, giving good agreement with the experiment in terms of magnitude and slope ($\Delta C_L/C_\mu = 44.4$). CFD does however over predict the lift increment at the higher momentum coefficient ($C_\mu = 0.06$), though this was also reported by Englar et al.,[13] Jones et al.,[43] and by Thomas [40], and was attributed to deficiencies in the turbulence modelling.

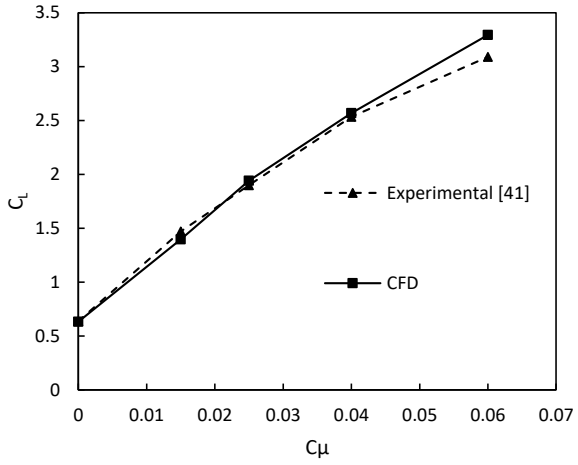

Fig. 8 C_L **vs.** C_μ **at** M_∞ **= 0.1, unsteady SA model, AoA =** $0°$**, time step = 0.001s. Compared with experimental data.**

Fig. 9 presents the pressure coefficient distribution over the aerofoil surface for $C_\mu = 0.06$. The CFD data agrees well with experiment on both the upper and lower surfaces, including the peak suction value around the Coanda surface.

On the lower surface there is a small discrepancy with experiment that results in the over-prediction of lift observed in Fig. 8. This might also be explained by the small pressure peak that was measured near the trailing edge due to issues with the experimental data [41].

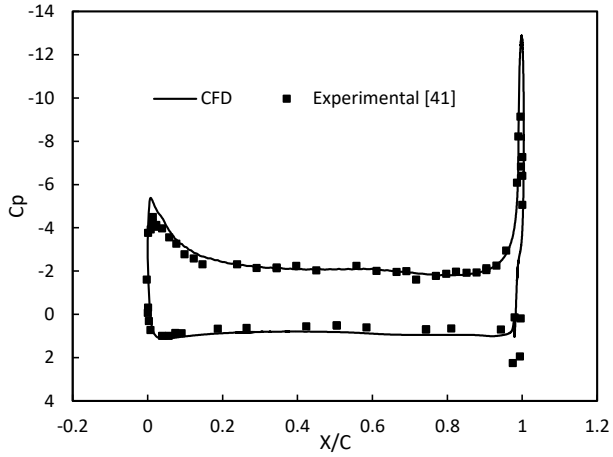

Fig. 9 The wing surface distribution of pressure coefficient at $C_\mu = 0.06$, compared with experimental data.

Fig. 10 presents the variation of C_L with AoA for three different momentum coefficients. In general CFD is in good agreement with experiment except at higher AoA (both positive and negative) where CFD over-predicts the lift increment. For example at AoA = 0°, the maximum deviation from experimental data is $\Delta C_{Lmax} = 0.11$, which increases to $\Delta C_{Lmax} = 0.23$ at AoA = -6° . Fig. 11 illustrates the velocity vectors at the nozzle exit and at the rear stagnation (separation) point around the Coanda trailing-edge. At the nozzle exit the jet is relatively thin with a non-uniform velocity profile. The jet flow remains attached to the Coanda surface for a significant distance causing a rotation of the external flow that it entrains. The attached boundary-layer becomes thicker as it decelerates around the trailing-edge before finally separating from the surface.

III. Unsteady validation

A step response is frequently used for analysing the dynamic characteristics of a system. For GLA we are interested in an aerofoil's step response to a sharp edge gust [44–46] i.e. a sudden vertical velocity component that changes the angle of attack[47] For example, consider an aircraft that is initially flying in a quasi-steady state in calm air, that encounters a uniform vertical gust with velocity of w_g - the interface between the calm air region and the gust region is a step change in velocity. Although an ideal sharp edge gust is not realizable in actual flight or in a wind tunnel, it can be studied by analytical methods or CFD simulations to understand the time history of incremental lift after it encounters the gust. Analytical solutions for this lift response have been derived by Hans Georg Küssner [48, 49], and are used here to validate the unsteady CFD simulations. Küssner developed an exponential equation 5 for a flat plate experiencing a

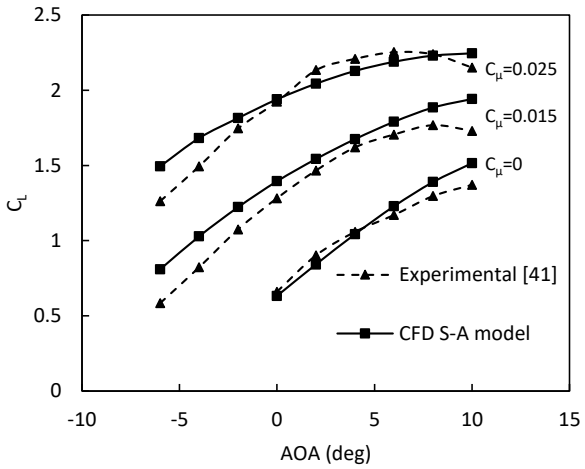

Fig. 10 C_L **vs. AOA in different blowing momentum coefficient at** M_∞ **= 0.1. Compared with experimental data.**

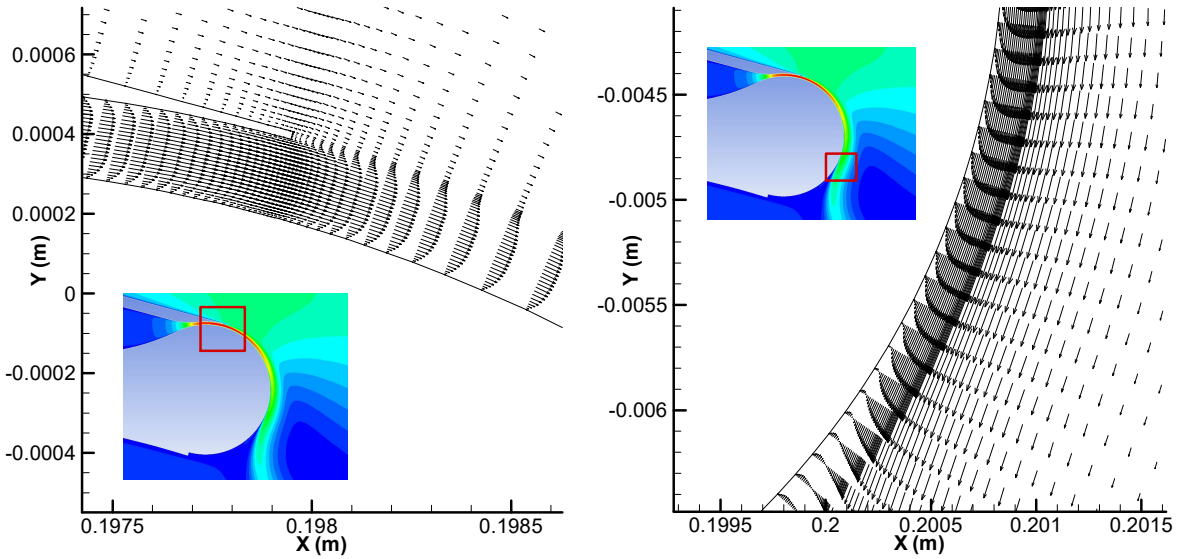

Fig. 11 The velocity profiles on the trailing edge at $C_\mu = 0.015$**,** M_∞ **= 0.1, left: nozzle exit, right: separation point on the round trailing edge.**

unit step gust in an incompressible flow. The function was extended from a theory of non-uniform motion of a thin aerofoil in potential flow initially given by Wagner [49].

$$\Psi(s) = 1 - 0.5e^{-0.13s} - 0.5e^{-s} \tag{5}$$

In this equation, $\Psi(s)$ is the lift variation with nondimensional distance travelled, $s = 2U * t/c$, over the time period t. Note the coefficients may have been modified slightly by other references [50–52], but this study has adopted the coefficients approximated by William Sears et al. [53].

Although the Küssner function is derived for a thin flat plate, theoretically a thin symmetrical aerofoil should also give similar results since the function is based on thin aerofoil theory [54]. A NACA0012 aerofoil was selected for the unsteady validation with a unit chord. Fig. 12 shows the structured mesh generated using the Pointwise software, which has 807,000 cells with a circular-shaped domain, dimensioned so that the far-field boundary is 10c from the aerofoil (noting that from the steady validation case we might expect a 0.5% lower C_L compared to the 100c far field). There are 808 points around the aerofoil and 1001 points in the wall normal direction. In the wall normal direction, the thickness of each mesh layer is gradually increased from 1×10^{-5}m at the aerofoil surface to a distance 0.01m from the surface. Beyond this the edge length is kept uniform to ensure a relatively fine mesh in the freestream flow to reduce numerical dissipation of the gust front. The final mesh has a wall $y+$ value less than 0.7 and a convective courant number less than 0.3.

Although the previous GACC aerofoil was meshed using ICEM software, the mesh for the NACA0012 aerofoil was generated by Hyperbolic Extrusion using Pointwise software. In this approach, a marching front could be extruded from the wing surface to the farfield. Despite the non-uniform distribution of points on the aerofoil surface, the Hyperbolic Extrusion method produces a high quality orthogonal mesh, and a smooth transition from a high to low density region to capture the propagating front, and avoids high aspect ratio cells near the farfield relative to the previous mesh strategy (since the block topology used in ICEM is more suited for complex geometries). For both cases, similar parameters (including first layer thickness, growth rates, point distribution over the aerofoil surface, and algorithm) were used for the near wall region in order to achieve consistency between the two mesh approaches.

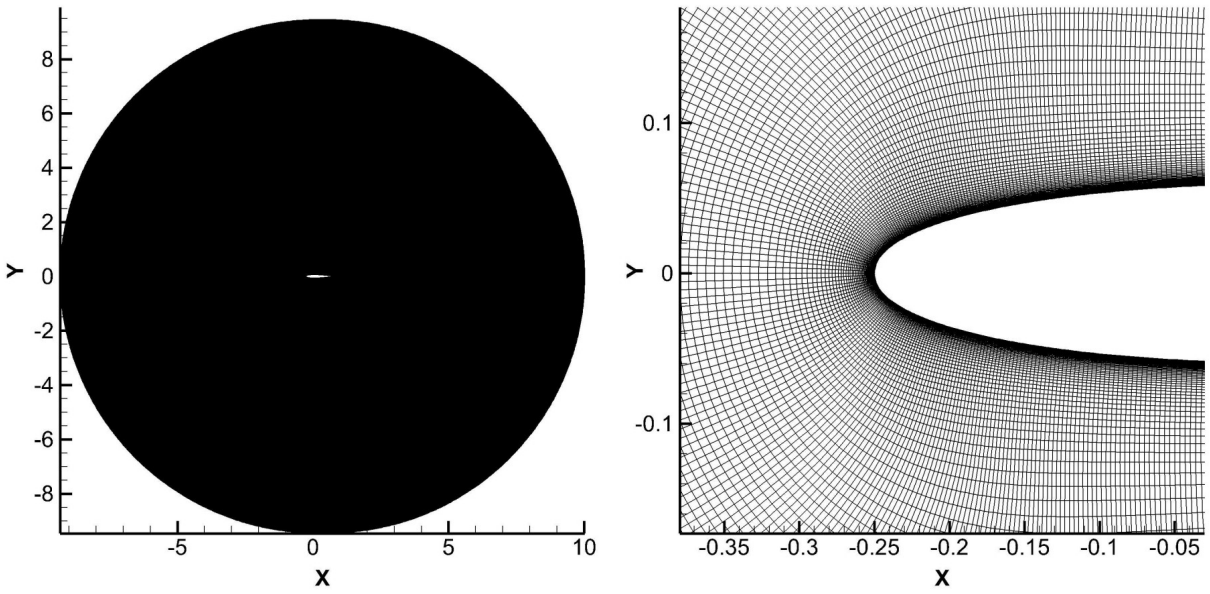

Fig. 12 The computational mesh for unsteady validation of NACA0012 aerofoil, left: the computational domain with a uniform density from the aerofoil to the farfield, right: the mesh distribution near the wall.

A sharp edge gust is realized by applying an initial vertical velocity component to every cell in a specific field ahead of the aerofoil [39, 55, 56], or by imposing an unsteady gust profile on the inflow boundary [54]. The first method may cause convergence issues due to the discontinuity at the interface and is not available in most solvers. The second method is easily realizable but the gust front may be smeared due to numerical dissipation as the gust front travels from the inflow boundary to the leading edge of the aerofoil. In this study the latter approach was used, with a high mesh density upstream of the aerofoil to reduce numerical dissipation, and a user-defined function (UDF) that specifies a vertical gust front at the inflow boundary. Since this boundary has a circular shape, the gust front passes each element on the boundary at a different time, determined by the UDF. Thus, assuming x is the cell centre on the X axis, the vertical velocity component of each face on the boundary is controlled using the function;

$$w_g(t) = \begin{cases} 0, & (t - t_0) < (x - x_0)/u \\ w_0, & (t - t_0) \geq (x - x_0)/u \end{cases} \tag{6}$$

where x_0 is the initial position of the gust front which is on the far left of the computational domain, t_0 is the time when the gust starts moving, w_0 is the vertical component of the gust velocity, u is the free stream velocity. This function is actually a criterion to evaluate when the gust front passes each cell. Fig. 13 displays an instantaneous vertical velocity distribution that clearly shows the gust front located at x = -5.5m, as it travels from left to right. On the left side, a uniform vertical gust velocity $w_g = 1m/s$ is applied, whilst on the right side the vertical velocity is zero. Simulations were performed for 2 streamwise velocities, U_∞ = 34m/s (M_∞ = 0.1) and U_∞ = 68m/s (M_∞ = 0.2), giving a chord Reynolds number, Re = 2.31×10^6 and 4.62×10^6 respectively. At t = 0, the initial position of the gust front is x = -10m. The penetration speed of the gust is the same as the free stream velocity, U_∞.

Unsteady simulations were initialised from a fully converged simulation with steady boundary conditions (U_∞ = 34m/s or U_∞ = 68m/s, AoA = 0°, T = 288K), prior to the UDF being used to create the gust front. As the gust front passes the aerofoil, a time history of C_L is recorded and compared with analytical results. Fig. 14 gives the unsteady validation results for both M_∞ = 0.1 and M_∞ = 0.2 cases. Simulated results are in very good agreement with analytical solutions as well as simulated results from other researchers. Note there is a small lag compared with the analytical curve due to numerical dissipation. Considering two adjacent cells in the flow domain, since the velocity components are defined at the centroid, the discretization scheme will create a gradient over the distance between the two centroids, so a perfectly sharp edge is not achievable except for some custom codes [39]. Consequently it is difficult to determine the exact time when the gust front arrives at the leading edge, and it is assumed to correspond to the time when C_L increases to 5% above the steady state value (C_{Lss}), leading to a small inaccuracy in the interaction time and the lag that was observed compared with analytical results. In the horizontal axis, $s = 2t * U/c$ is the nondimensional time in terms of the half chord, which is used in the derivation of the Küssner function. However, in some of the following

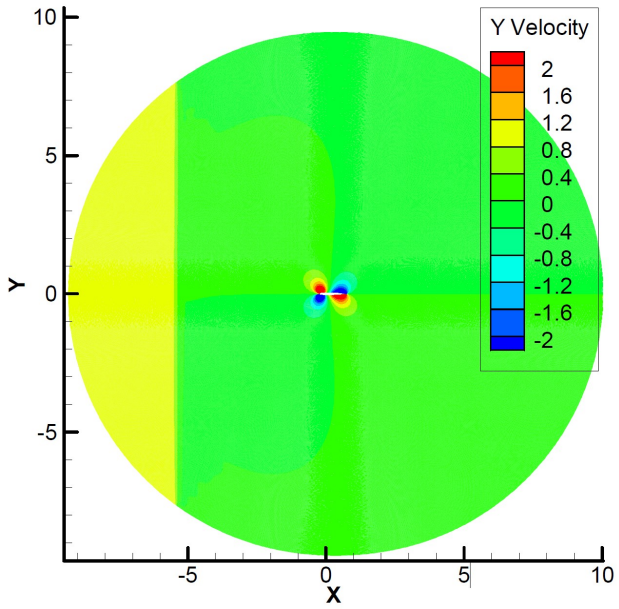

Fig. 13 The vertical velocity field showing the gust front marching from left side of the domain.

figures, $s' = t * U/c$ is also used when Küssner's curve is absent, since chord length is usually used as a reference length for fluid dynamics.

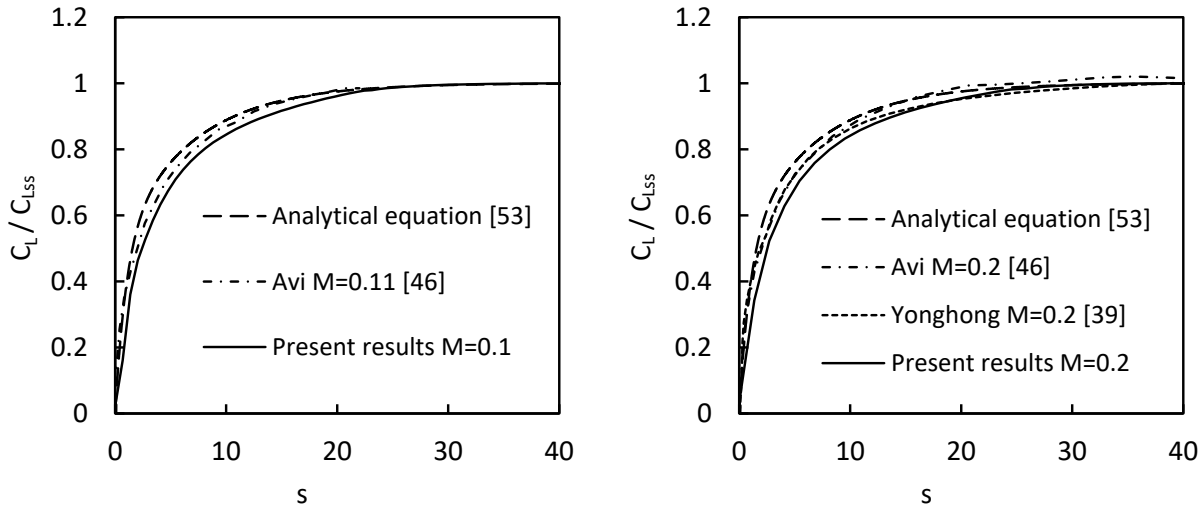

Fig. 14 Unsteady validation results of the NACA0012 aerofoil encountered a sharp edge gust, left: M_∞ = 0.1, right: M_∞ = 0.2.

IV. Study of the CC dynamic response

A. Lift response to a dynamic CC input

Since the present study concerns the control of unsteady lift behaviour during vertical gusts, an understanding of the dynamic characteristics of circulation control is essential to develop a suitable control system. Typically the dynamic characteristics of conventional (mechanical) control surfaces are obtained in sub-scale wind tunnel tests to measure hinge-moments in order to size actuators. Note the actuation with respect to pneumatic control is by means of varying the NPR. Actuator dynamic response will be evaluated for steady and unsteady load cases to derive a numerical model that can be used in the control algorithm design. The dynamic lift response to NPR changes can be evaluated using CFD with a periodic boundary condition to vary the plenum chamber stagnation pressure and therefore NPR. Since the control design requires accurate response data, the time-step settings in the transient solver were examined to ensure that the temporal variations of lift are physical i.e. the time step must be small enough to ensure a stable time accurate solution and that the frequency and associated physics are resolved. A time-step independence study was performed specifying a sinusoidal plenum chamber stagnation pressure with a 10 Hz frequency and an amplitude range of 0 - 20kPa (gauge pressure), with 10 inner iterations per time step.

Fig. 15 shows the C_L response with time for time-steps in the range 0.01ms to 5ms, with the periodic NPR starting after 0.5s. Clearly with a time-step greater than 0.5ms it is not possible to capture the physical response, whereas for a time-step less than 0.1ms the response is adequately captured and is independent of the time step. Consequently a time-step of 0.1ms was selected for all further calculations, which gives a reasonable computational expense (i.e. 12s simulation time requires 22 hours of elapsed computing time running on an HPC with 8 cores).

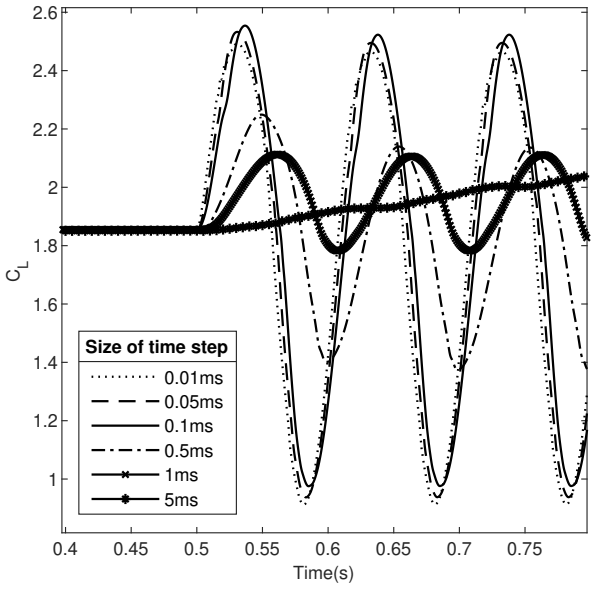

Fig. 15 Simulated lift coefficient response with different time steps.

B. Variation of the flow field for step input

Based on the validated solver settings, an unsteady simulation for a step response was performed. The variation of the flow field for the initial 0.01s is captured and shown in Figure 16. Prior to t = 0 the solver was run for 10,000 time steps without blowing to achieve a converged and stable flow field. At t = 0s, a total pressure of 10kPa is applied to the nozzle inlet. Then at t = 0.001s the high-pressure flow is discharged to the external flow through the nozzle and immediately attaches to the circular Coanda surface. From t = 0.001s to 0.01s the Coanda jet remains attached and the rear stagnation point moves clockwise around the surface. As a result the external pressure distribution is changed and a suction peak appears upstream of the nozzle exit during this period. The results show that the plenum chamber flow and the attachment of the Coanda jet were accomplished very quickly in 0.01s, equivalent to $s' = 1.7$.

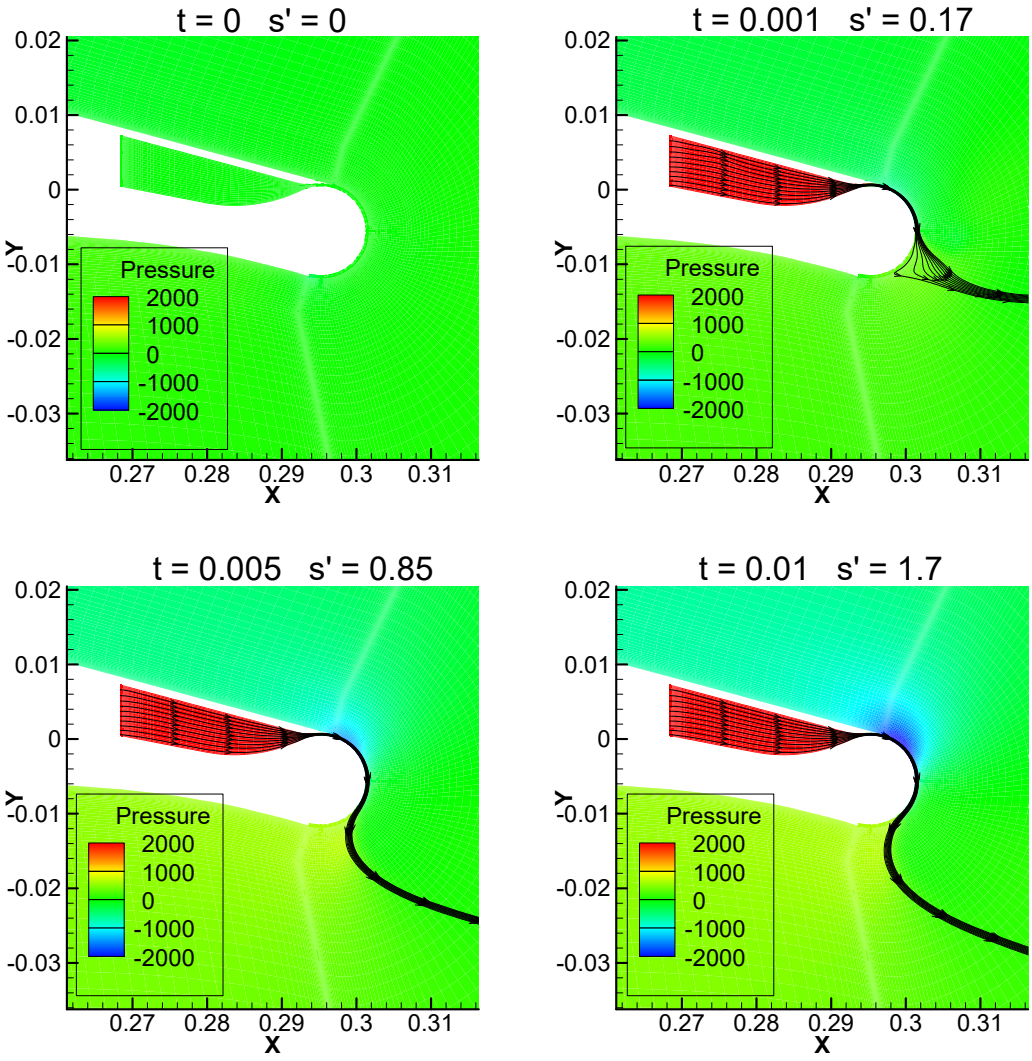

Fig. 16 Flow field variation after a step input, t = physical time in seconds, s' = nondimensional time.

C. Comparison of the response of CC and mechanical ailerons

The dynamic response of mechanical control surfaces depends on the actuation speed of servo motors. A typical servo motor has a time constant of the order of 0.1s [1]. This is sufficient to damp the short-period mode but not able to alleviate gust loading that has a higher frequency. A fast-actuation effector developed by Elisa and Israel[34] had a maximum deflection rate of approximately $300°/s$. Consequently this control surface could potentially be used to compensate high frequency gusts. Fig. 17 shows their experimental rig of a NACA 0021 aerofoil with a flap driven by a pneumatic cylinder giving a maximum deflection angle of 30°. This experimental result has been compared with the GACC aerofoil in terms of lift response to a rapid actuation.

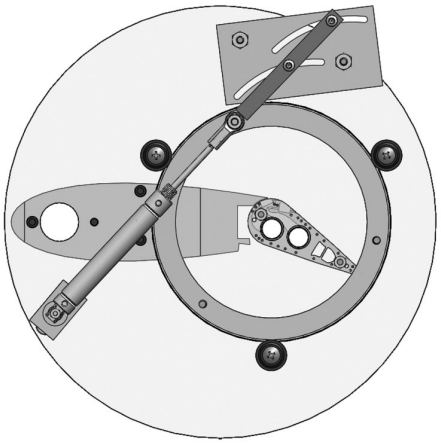

Fig. 17 The experimental rig for a fast-actuation flap [34]. (Reprinted with permission from the American Institute of Aeronautics and Astronautics. Copyright © 2012 by the American Institute of Aeronautics and Astronautics, Inc.)

Fig. 18 compares the simulated lift response to a step input from the present study (GACC aerofoil with a pneumatic flap), with the measured results for a mechanical flap reported in [34], where C_{Lss} is the steady state value after the flow has stabliszed. Due to the inertia of a mechanical flap mechanism it is not possible to rotate a mechanical flap instantaneously. In the experiments reported by Elisa and Israel [34], three actuation speeds were presented for Re = 200,000 (U_∞ = 10 m/s), with a fast actuation taking $s' \approx 2.67$ to complete a 30° rotation, a medium actuation taking $s' \approx 3.67$ and a slow actuation taking $s' \approx 5.33$. The three vertical dashed lines in Fig. 18 denote these times for the mechanical flap to fully rotate 30° and then be suddenly halted by a stopper [34]. Simulated results assume an instantaneous change to NPR since, by contrast, the opening of a valve to control the plenum pressure can be less than 0.5ms ($s' = 0.085$)[57]. The initial rate of increase in C_L is higher for the pneumatic flap compared to the mechanical flap, but both systems achieve 95% of the steady state C_L in $s' \approx 7$.

The simulated response at a higher Re number, Re = 460,000 (U_∞ = 34m/s), is shown in Fig. 19 for the GACC aerofoil, plotted as a function of physical time rather than nondimensional time. Since no experimental data was

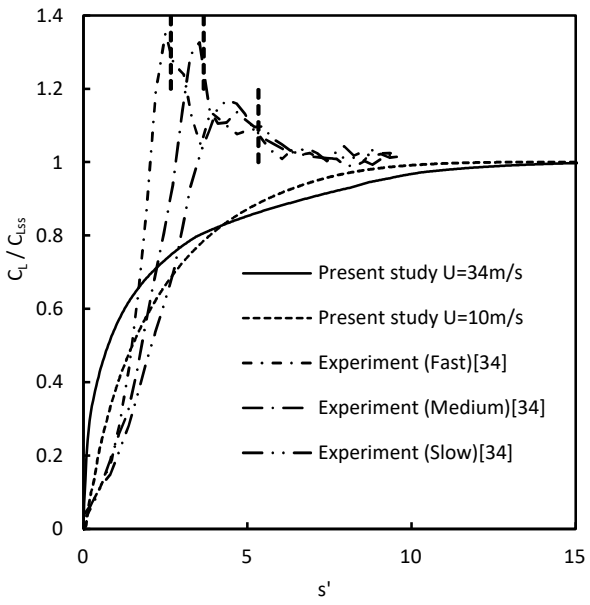

Fig. 18 Lift response to a step input for circulation control in the present study and a mechanical plain flap from experiments[34].

available at this condition it was assumed that the mechanical flap could maintain the deflection rate of $300°/s$ at the higer freestream speed, though the increased aerodynamic loading may reduce this rate. Plotted against physical time the difference between the GACC and mechanical flap is more apparent. In addition, the step response of typical actuators on aircraft in operation is also plotted as a grey area in Fig. 19, which will be explained later. For the GACC aerofoil the step response is faster at the higher freestream velocity. Recalling that the time from valve opening to the formation of a jet flow was completed in 0.001s (as shown in Fig. 16), which is relatively small. Most of the actuation time is attributed to the response of the surrounding fluid until a quasi steady state is achieved. For different free stream velocities, this fluidic response is nearly constant in terms of s', but the physical time is reduced at the higher freestream velocity. In contrast, the mechanical flap rotation rate is assumed to be unaffected by freestream velocity, or slower in a higher freestream velocity, in terms of physical time.

According to Theodorsen's research [58], the unsteady lift response to an arbitrary motion of the flap is the summation of circulatory lift and non-circulatory lift. The former is the lift due to a change in circulation of the aerofoil, including the presence of a dynamic stall vortex (DSV). The latter can be formed by the displacement of the surrounding fluid due to a rapid flap deflection as the fluid around the flap is accelerated, and tends to increase the hinge moment. Although the net circulation does not change, a temporary increase in lift is observed named non-circulatory lift [59]. Circulatory lift is a function of nondimensional time s', and if the circulation of an aerofoil changes abruptly the time history curve of lift can be approximated as a Wagner function [58]. This function is independent of aerofoil geometry and Reynolds number, and assumes a potential and incompressible flow. In comparison, the dynamic response of

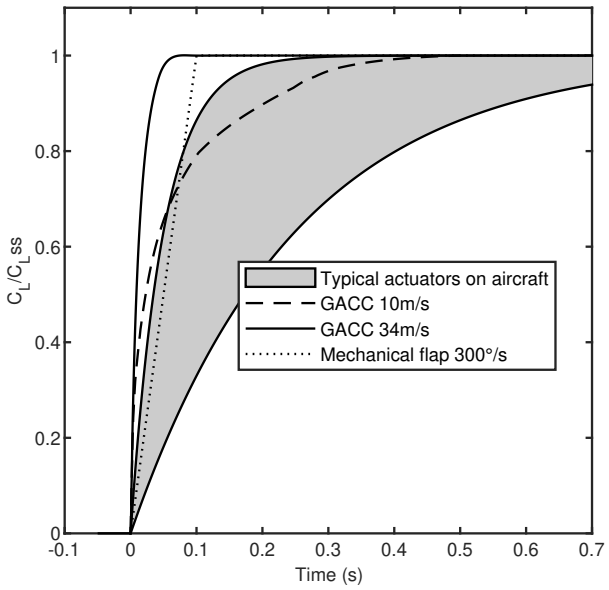

Fig. 19 Comparison of lift response to a step input over physical time.

non-circulatory lift depends on the size of aerodynamic surfaces, rotation rate and acceleration. A mechanical flap that is turning downward will generate an additional positive lift. It may also create a DSV which passes over the upper surface of the flap creating a temporary increase in lift, as shown in Fig. 18. In order to evaluate the dynamic performance of GACC and mechanical flaps, we can analyse the time when it reaches a steady state. This 'settling' time (when the lift reaches 95% of the steady state value) depends on the slowest component of circulatory or non-circulatory lift. For a mechanical flap, settling time is always longer than the time of flap rotation, when the flap reaches the desired position and stops, the fluid needs additional time to settle down. This is clearly shown in Fig. 18. In addition, a set of analytical equations provided by Gordon Leishman [50] can solve the time history value of C_L due to arbitrary flap motion. Unlike mechanical flap, the GACC aerofoil is equivalent to an infinitely small flap located at the trailing edge of the aerofoil. It can change the rear stagnation point abruptly ($s' < 1$, Fig. 16) without adding non-circulatory lift or DSV as there is no moving part on the aerofoil, the lift response is just a function of convective time s'. As a result, the settling time of GACC is shorter than a mechanical flap at U_∞ = 34m/s or at a higher velocity.

Note the deflection rate of 300°/s is a relatively fast actuation rate found in the reference [34]. However in practice, the angular rate of aerodynamic surfaces on aircraft are usually slower. Most of the mechanical aerodynamic surfaces are linked to servo motors which can be modelled by first-order systems, assuming the transfer function is $G(s) = 1/(\tau s + 1)$, their time constant τ is in the range of 0.05 -0.25 [1]. The step response of a typical first-order system reaches 95% of its steady state value at $t = 3\tau$. Corresponding to angular rate 40°/s – 200°/s, assuming the maximum deflection angle is 30°, the step response within this range is plotted in Fig. 19 as a grey area which falls behind GACC aerofoil. The settling time of mechanical flap is equivalent to nondimensional time $s' = 17$ to 85. This compares with a settling time

of around $s' = 7 - 9$ for the GACC aerofoil which is even faster at higher freestream velocity without any mechanical limitation or hinge loading effects.

Another interesting finding is that the lift response of the GACC due to a step change in nozzle pressure is surprisingly close to the Küssner function, shown in Fig. 20. However the Küssner function describes a sharp edge gust passing over a thin flat plate, which is a different scenario to the GACC aerofoil. This is probably because the sudden actuation of blowing jet on a GACC aerofoil changes the boundary condition of the aerofoil, while the gust passing over a flat plate can be regarded as a sudden change in angle of attack, based on Küssner's theory. In both scenarios, the settling time is fundamentally how fast the flow converged to a steady state. Discarding the difference in boundary conditions, the steady state of both scenarios is similar as their Mach number, Reynolds number and steady state C_L are the same. Therefore it is possible to use the Küssner function to describe a dynamic process for circulation control. This also indicates that the lift response of GACC to unsteady nozzle inputs is not a simple first order system, but it is likely to be a third order system like the Küssner function. In addition, the Wagner function (Equation 7) is also plotted in Fig. 20. Wagner function describes lift response to a step change in AoA for a flat plate [50]. This function also has a similar shape compared to GACC results except for the nonzero initial conditions ($\phi(s = 0) = 0.5$). The initial condition is noncirculatory dominated due to displacement of surrounding air caused by indicial motion [50]. However there are no moving parts in a GACC aerofoil and the lift is mainly caused by circulation, which means the initial condition of GACC is different from Wagner function. Friedman and Arieli have reported a similar comparison between the lift response of circulation control and Wagner function [38], results showed a good correlation, but not as close as the Küssner function.

$$\phi(s) = 1 - 0.2048e^{-0.0557s} - 0.2952e^{-0.333s} \tag{7}$$

A further analysis was performed considering different input frequencies and amplitudes for the plenum stagnation pressure to determine the frequency response. In the CFD simulation of this aerofoil, the input variable is the nozzle pressure and the output is lift. However, when analysing the bandwidth of CC, it is more convenient to compare the magnitude ratio between the dynamic C_L (with sinusoidal blowing) and the quasi steady $C_{L_{ss}}$. Which gives an intuitive comparison about how the magnitude of C_L reduces with higher frequency. The relationship of nozzle pressure and $C_{L_{ss}}$ at steady state is given by:

$$C_{L_{ss}} = f(C_\mu) \tag{8}$$

The $f(C_\mu)$ is the steady-state lift response to different nozzle pressures and can be obtained from Fig. 8, according to the steady state CFD simulations. Fig. 21 shows a Bode diagram of the dynamic results, where the output magnitude is defined as the ratio between the magnitude of sinusoidal output C_L and the quasi-steady $C_{L_{ss}}$, given in decibels. Only the oscillatory component of lift is used in the Bode plot. A frequency range from 3.14 to 314 rad/s and input amplitudes of ±1kPa and ±10kPa were considered. In addition, a freestream Mach number $M_\infty = 0.2$ was also considered with an

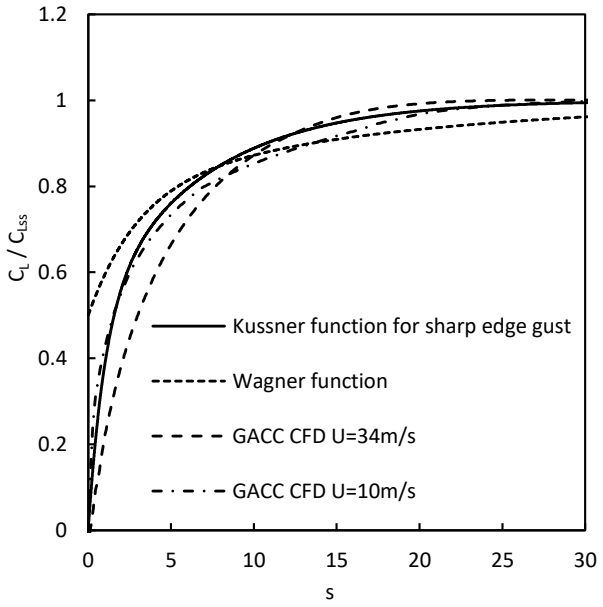

Fig. 20 Comparison of the lift response of GACC aerofoil to a step input and the Küssner and Wagner function.

amplitude of ±1kPa. The response of a mechanical flap governed by a first order transfer function is also plotted for comparison, using the same assumptions as in Fig. 19.

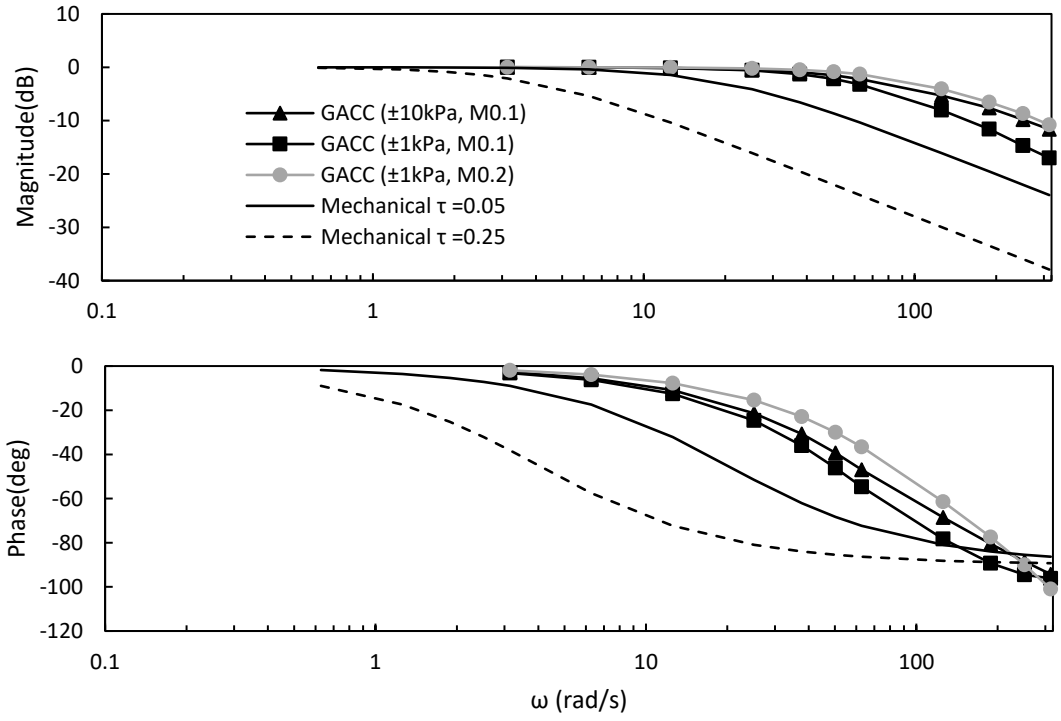

Fig. 21 Comparison of amplitude and phase response with different nozzle pressure range and velocity.

Fig. 21 shows the dynamic performance of the GACC aerofoil is significantly better than mechanical flaps. When the magnitude of the lift response reduces to -3dB (0.707 of the quasi-steady value), the mechanical flap is in the range of 4-20 rad/s compared with the GACC at 60-101 rad/s. In terms of the phase lag, the mechanical flap reaches -45° in the range of 53-77 rad/s, compared with GACC at 90-97 rad/s. The higher bandwidth of CC means that it can be used in some scenarios that require fast actuation, for example gust alleviation or flutter control, though in practice, the bandwidth of CC may be limited by the actuation speed of a pneumatic valve [9, 10]. However, it is much easier to increase the bandwidth of a valve than an aerodynamic surface which has a much stronger aerodynamic load. Additionally, it is found that the amplitude response of a stronger fluctuation ($\pm 10kPa$) is faster than a smaller fluctuation ($\pm 1kPa$). The cause of this response is still unknown, and further study is needed. Also, a higher free stream Mach number ($M_\infty = 0.2$) gives a faster response than a lower Mach number ($M_\infty = 0.1$). This can be explained by the previous observation that the response of GACC is actually the settling response of the surrounding fluid which is highly dependent on the free stream velocity.

Some high-bandwidth mechanical actuators, for example a piezoelectric tab [60], can actuate as fast as 300Hz. Although it actuates faster than the CC, its ability to change lift is much smaller than a plain flap and significantly less than CC, since piezoelectric tabs can only deflect for a few degrees. The incremental lift coefficient that can be generated by deflecting a plain flap (or aileron) is typically less than 1 [61]. By comparison CC provides large lift augmentation of up to $\Delta C_L = 9$ [8]. Since any rapid flap deflection modifies lift by increasing camber, their influence on the external flow should still follow Wagner's theorem except when the flap is sub-boundary layer, in which case it couldn't be assumed as potential flow, and Wagner's theorem is invalid.

V. Conclusion

This paper has considered active circulation control (CC) as a means of increasing the actuation bandwidth for gust load alleviation compared with a conventional mechanical flap. A CFD validation of the general aviation circulation control aerofoil showed that lift and pressure coefficient data predicted by steady CFD was consistent with the experiment. Further unsteady validation presented good agreement with analytical results. The dynamic characteristics were then investigated for a sinusoidal plenum chamber pressure using transient CFD (URANS) simulations. By varying the frequency and magnitude of the sinusoidal chamber pressure, the frequency response was obtained. The dynamic characteristics of CC were also compared with a conventional mechanical flap and the actuation speed of CC was found to be approximately twice as fast as a typical mechanical actuator when $U_\infty = 34$m/s. In terms of frequency response, the max bandwidth of CC at the magnitude of -3dB is 101 rad/s, which is 5 times faster than a typical mechanical actuator. The $-45°$ phase lag of CC is 97 rad/s, which is approximately twice as fast. The comparison between CC and mechanical flaps indicates that CC can be used as a high bandwidth, low lag actuator for gust alleviation applications. The second part of this research will describe the implementation of CC in a closed-loop gust alleviation system, which

will be presented in a separate paper.

Acknowledgments

The author gratefully acknowledges the funding received towards my PhD from the China Scholarship Council.

References

[1] Nelson, R. C., et al., *Flight stability and automatic control*, Vol. 2, WCB/McGraw Hill New York, 1998.

[2] Arjomandi, M., Agostino, S., Mammone, M., Nelson, M., and Zhou, T., "Classification of unmanned aerial vehicles," *Report for Mechanical Engineering class, University of Adelaide, Adelaide, Australia*, 2006.

[3] Cook, M. V., *Flight dynamics principles: a linear systems approach to aircraft stability and control*, Butterworth-Heinemann, 2012, p. 457.

[4] Hahn, K.-U., and König, R., "Advanced technologies testing aircraft system flight test and simulation results of the advanced gust management system LARS," *Guidance, Navigation and Control Conference*, 1992, p. 4343. https://doi.org/10.2514/6.1992-4343.

[5] Cates, M. C., Paranto, J. N., and Larsen, T. A., "Multifunction aircraft Light Detection and Ranging (LIDAR)," , Aug. 13 2013. US Patent 8,508,721.

[6] Walton, V. M., Borland, C. J., Siu, T. L., Najmabadi, K., Coleman, E. E., Marquis, D. P., McMullin, D. L., and Milligan, K. H., "Vertical gust suppression system for transport aircraft," , Jul. 8 2014. US Patent 8,774,987.

[7] McGowan, G., Gopalarathnam, A., and Jones, G., "Analytical and computational study of adaptive circulation control airfoils," *22nd Applied Aerodynamics Conference and Exhibit*, 2004, p. 4721. https://doi.org/10.2514/6.2004-4721.

[8] Golden, R., and Marshall, D., "Design and performance of circulation control flap systems," *48th AIAA Aerospace Sciences Meeting Including the New Horizons Forum and Aerospace Exposition*, 2010, p. 1053. https://doi.org/10.2514/6.2010-1053.

[9] Buonanno, A., "Aerodynamic circulation control for flapless flight control of an unmanned air vehicle," 2009.

[10] Buonanno, A., and Cook, M., "Flight dynamic simulation of a flapless flight control UAV," *25th International Congress of the Aeronautical Sciences*, 2006.

[11] Savvaris, A., Buonanno, A., Jamil, R., and Tsourdos, A., "Design and development of the DEMON UAV fluidic flight control system," *AIAA Infotech@ Aerospace (I@ A) Conference*, 2013, p. 4820. https://doi.org/10.2514/6.2013-4820.

[12] Yang, Z., Igarashi, H., Martin, M., and Hu, H., "An experimental investigation on aerodynamic hysteresis of a low-Reynolds number airfoil," *46th AIAA aerospace sciences meeting and exhibit*, 2008, p. 315. https://doi.org/10.2514/6.2008-315.

[13] ENGLAR, R., JONES, G., Allan, B., and Lin, J., "2-D circulation control airfoil benchmark experiments intended for CFD code validation," *47th AIAA Aerospace sciences meeting including the new horizons forum and aerospace exposition*, 2009, p. 902. https://doi.org/10.2514/6.2009-902.

[14] Cagle, C., "A wind tunnel model to explore unsteady circulation control for general aviation applications," *22nd AIAA Aerodynamic Measurement Technology and Ground Testing Conference*, 2002, p. 3240. https://doi.org/10.2514/6.2002-3240.

[15] Swanson, R., Rumsey, C., and Anders, S., "Progress towards computational method for circulation control airfoils," *43rd AIAA Aerospace Sciences Meeting and Exhibit*, 2005, p. 89. https://doi.org/10.2514/6.2005-89.

[16] Rogers, E., and Donnelly, M., "Characteristics of a dual-slotted circulation control wing of low aspect ratio intended for naval hydrodynamic applications," *42nd AIAA Aerospace Sciences Meeting and Exhibit*, 2004, p. 1244. https://doi.org/10.2514/6.2004-1244.

[17] Paschal, K., Neuhart, D., Beeler, G., and Allan, B., "Circulation control model experimental database for CFD Validation," *50th AIAA Aerospace Sciences Meeting including the New Horizons Forum and Aerospace Exposition*, 2012, p. 705. https://doi.org/10.2514/6.2012-705.

[18] Englar, R., "Circulation control pneumatic aerodynamics: blown force and moment augmentation and modification-Past, present and future," *Fluids 2000 Conference and Exhibit*, 2000, p. 2541. https://doi.org/10.2514/6.2000-2541.

[19] Kanistras, K., Saka, P. C., Valavanis, K. P., and Rutherford, M. J., "Wind Tunnel Investigation of a Circulation Control Wing with Dual-Radius Flaps," *Journal of Aircraft*, Vol. 55, No. 4, 2018, pp. 1731–1741. https://doi.org/10.2514/1.C034208.

[20] Miklosovic, D., Imber, R., and Britt-Crane, M., "Measurements of Midspan Flow Interactions of a Low-Aspect-Ratio Circulation Control Wing," *Journal of Aircraft*, Vol. 53, No. 6, 2016, pp. 1969–1974. https://doi.org/10.2514/1.C033852.

[21] Hoholis, G., Steijl, R., and Badcock, K., "Circulation Control as a Roll Effector for Unmanned Combat Aerial Vehicles," *Journal of Aircraft*, Vol. 53, No. 6, 2016, pp. 1875–1889. https://doi.org/10.2514/1.C033642.

[22] Traub, L. W., and Biegner, M., "Experimental Evaluation of a Self-Contained Circulation-Control Wing," *Journal of Aircraft*, Vol. 50, No. 3, 2013, pp. 764–777. https://doi.org/10.2514/1.C031937.

[23] Li, Z., Liu, Y., Zhou, W., Wang, S., Wen, X., and Liu, Y., "Lift Augmentation Potential of the Circulation Control Wing Driven by Sweeping Jets," *AIAA Journal*, Vol. 0, No. 0, 0, pp. 1–22. https://doi.org/10.2514/1.J061456.

[24] Xu, H.-Y., Qiao, C.-L., Yang, H.-Q., and Ye, Z.-Y., "Active Circulation Control on the Blunt Trailing Edge Wind Turbine Airfoil," *AIAA Journal*, Vol. 56, No. 2, 2018, pp. 554–570. https://doi.org/10.2514/1.J056223.

[25] Itsariyapinyo, P., and Sharma, R. N., "Experimental Study of a NACA0015 Circulation Control Airfoil Using Synthetic Jet Actuation," *AIAA Journal*, Vol. 60, No. 3, 2022, pp. 1612–1629. https://doi.org/10.2514/1.J060508.

[26] Bagheri, A. K., Jones, D. P., and Gaitonde, A. L., "Linear Reduced-Order Model of Airfoil Gust Response," *Journal of Aircraft*, Vol. 56, No. 3, 2019, pp. 1264–1271. https://doi.org/10.2514/1.C035011.

[27] Wales, C., Gaitonde, A., and Jones, D., "Reduced-Order Modeling of Gust Responses," *Journal of Aircraft*, Vol. 54, No. 4, 2017, pp. 1350–1363. https://doi.org/10.2514/1.C033765.

[28] Zhao, Y., Yue, C., and Hu, H., "Gust Load Alleviation on a Large Transport Airplane," *Journal of Aircraft*, Vol. 53, No. 6, 2016, pp. 1932–1946. https://doi.org/10.2514/1.C033713.

[29] Carlsson, M., "Control surface response of a blended wing body aeroelastic wind-tunnel model," *Journal of aircraft*, Vol. 42, No. 3, 2005, pp. 738–742. https://doi.org/10.2514/1.5440.

[30] Ghoreyshi, M., and Cummings, R. M., "Unsteady aerodynamic modeling of aircraft control surfaces by indicial response methods," *AIAA journal*, Vol. 52, No. 12, 2014, pp. 2683–2700. https://doi.org/10.2514/1.J052946.

[31] Fonte, F., Ricci, S., and Mantegazza, P., "Gust load alleviation for a regional aircraft through a static output feedback," *Journal of Aircraft*, Vol. 52, No. 5, 2015, pp. 1559–1574. https://doi.org/10.2514/1.C032995.

[32] Seidler, R. B., Marten, S., Widhalm, M., and Wild, J., "Efficient Prediction of Aerodynamic Control Surface Responses Using the Linear Frequency Domain," *AIAA Journal*, Vol. 58, No. 5, 2020, pp. 1964–1975. https://doi.org/10.2514/1.J058840.

[33] Geisbauer, S., "Numerical Simulation and Validation of Aerodynamics of Static and Dynamic Spoilers," *Journal of Aircraft*, Vol. 58, No. 6, 2021, pp. 1187–1203. https://doi.org/10.2514/1.C036145.

[34] Phillips, E., and Wygnanski, I., "Use of sweeping jets during transient deployment of a control surface," *AIAA journal*, Vol. 51, No. 4, 2013, pp. 819–828. https://doi.org/10.2514/1.J051683.

[35] Heinz, N., King, R., Höll, T., Wassen, E., and Thiele, F., "Numerical Investigation of Robust Closed-Loop Flow Control of a High-Lift Configuration," *5th Flow Control Conference*, 2010, p. 4967. https://doi.org/10.2514/6.2010-4967.

[36] Xiaoping, X., Xiaoping, Z., Zhou, Z., and Ruijun, F., "Application of active flow control technique for gust load alleviation," *Chinese Journal of Aeronautics*, Vol. 24, No. 4, 2011, pp. 410–416. https://doi.org/10.1016/S1000-9361(11)60048-4.

[37] Kerstens, W., Pfeiffer, J., Williams, D., King, R., and Colonius, T., "Closed-loop control of lift for longitudinal gust suppression at low Reynolds numbers," *AIAA journal*, Vol. 49, No. 8, 2011, pp. 1721–1728. https://doi.org/10.2514/1.J050954.

[38] Friedman, C., Arieli, R., and Levy, Y., "Lift build-up on circulation control airfoils," *Journal of Aircraft*, Vol. 53, No. 1, 2016, pp. 231–242. https://doi.org/10.2514/1.C033304.

[39] Li, Y., and Qin, N., "Airfoil gust load alleviation by circulation control," *Aerospace Science and Technology*, Vol. 98, 2020, p. 105622. https://doi.org/10.1016/j.ast.2019.105622.

[40] Economon, T. D., Milholen II, W. E., and Branch, C. A., "Parametric investigation of a 2-D circulation control geometry," *Configuration Aerodynamics Branch Research and Technology Directorate Submitted: August*, Vol. 7, 2008.

[41] Jones, G. S., Viken, S. A., Washburn, A. E., Jenkins, L. N., and Cagle, C. M., "An Active Flow Circulation Controlled Flap Concept for General Aviation Aircraft Applications," *1st Flow Control Conference*, 2002. https://doi.org/10.2514/6.2002-3157.

[42] Shires, A., and Kourkoulis, V., "Application of circulation controlled blades for vertical axis wind turbines," *Energies*, Vol. 6, No. 8, 2013, pp. 3744–3763. https://doi.org/10.3390/en6083744.

[43] Jones, G. S., Lin, J. C., Allan, B. G., Milholen, W. E., Rumsey, C. L., and Swanson, R., "Overview of CFD validation experiments for circulation control applications at NASA," *2008 International Powered Lift Conference; London;22-24 Jul. 2008; United Kingdom*, 2008.

[44] Raveh, D. E., "CFD-based models of aerodynamic gust response," *Journal of Aircraft*, Vol. 44, No. 3, 2007, pp. 888–897. https://doi.org/10.2514/1.25498.

[45] Zaide, A., and Raveh, D., "Numerical simulation and reduced-order modeling of airfoil gust response," *AIAA journal*, Vol. 44, No. 8, 2006, pp. 1826–1834. https://doi.org/10.2514/1.16995.

[46] KARAKAŞ, M., "Gust alleviation techniques and design methods of active aeroelastic wing," Ph.D. thesis, Istanbul Technical University, 2020.

[47] Medina, A., Ol, M. V., Mancini, P., and Jones, A., "Revisiting conventional flaps at high deflection rate," *AIAA Journal*, Vol. 55, No. 8, 2017, pp. 2676–2685. https://doi.org/10.2514/1.J055754.

[48] Küssner, H. G., "Zusammenfassender Bericht über den instationären Auftrieb von Flügeln," *Luftfahrtforschung*, Vol. 13, No. 12, 1936, pp. 410–424.

[49] Jones, R. T., "The unsteady lift of a wing of finite aspect ratio," Tech. rep., 1940.

[50] Leishman, J. G., "Unsteady lift of a flapped airfoil by indicial concepts," *Journal of Aircraft*, Vol. 31, No. 2, 1994, pp. 288–297. https://doi.org/10.2514/3.46486.

[51] Wright, J. R., and Cooper, J. E., *Introduction to aircraft aeroelasticity and loads*, Vol. 20, John Wiley & Sons, 2008. https://doi.org/10.2514/4.479359.

[52] von Karman, T. H., and Sears, W. R., "Airfoil theory for non-uniform motion," *Journal of the Aeronautical Sciences*, Vol. 5, No. 10, 1938, pp. 379–390. https://doi.org/10.2514/8.674.

[53] Sears, W. R., "On the reaction of an elastic wing to vertical gusts," *Journal of the Aeronautical Sciences*, Vol. 8, No. 2, 1941, pp. 64–67.

[54] Ghoreyshi, M., Greisz, I., Jirasek, A., and Satchell, M., "Simulation and modeling of rigid aircraft aerodynamic responses to arbitrary gust distributions," *Aerospace*, Vol. 5, No. 2, 2018, p. 43. https://doi.org/10.3390/aerospace5020043.

[55] Förster, M., and Breitsamter, C., "Aeroelastic prediction of discrete gust loads using nonlinear and time-linearized CFD-methods," *Journal of Aeroelasticity and Structural Dynamics*, Vol. 3, No. 3, 2015.

[56] Bartels, R. E., *Development, Verification and Use of Gust Modeling in the NASA Computational Fluid Dynamics Code FUN3D*, National Aeronautics and Space Administration, Langley Research Center, 2012.

[57] SMC, *SX10 High-speed 2 Port Valve*, SMC Pneumatics LTD, 2 2014.

[58] Theodorsen, T., and Mutchler, W., "General theory of aerodynamic instability and the mechanism of flutter," 1935.

[59] Taha, H. E., and Rezaei, A. S., "On the dynamics of unsteady lift and circulation and the circulatory-non-circulatory classification," *AIAA Scitech 2019 Forum*, 2019, p. 1853. https://doi.org/10.2514/6.2019-1853.

[60] Heinze, S., and Karpel, M., "Analysis and wind tunnel testing of a piezoelectric tab for aeroelastic control applications," *Journal of Aircraft*, Vol. 43, No. 6, 2006, pp. 1799–1804.

[61] Gudmundsson, S., *General aviation aircraft design: Applied Methods and Procedures*, Butterworth-Heinemann, 2013.